Hindawi Publishing Corporation
Advances in Materials Science and Engineering
Volume 2013, Article ID 789373, 16 pages
http://dx.doi.org/10.1155/2013/789373

Research Article

Parameters Controlling the Oxide Reduction during Sintering of Chromium Prealloyed Steel

Monika Hrubovčáková,[1] Eva Dudrová,[1] Eduard Hryha,[2] Margita Kabátová,[1] and Jarmila Harvanová[3]

[1] *Institute of Materials Research of SAS, Watsonova 47, 040 01 Košice, Slovakia*
[2] *Department of Materials and Manufacturing Technology, Chalmers University of Technology, Rännvägen 2A, 412 96 Göteborg, Sweden*
[3] *University of Veterinary Medicine and Pharmacy, Komenskeho 73, 041 81 Košice, Slovakia*

Correspondence should be addressed to Monika Hrubovčáková; mhrubovcakova@imr.saske.sk

Received 21 May 2013; Accepted 28 August 2013

Academic Editor: Jörg M. K. Wiezorek

Temperature intervals of oxide reduction processes during sintering of the Fe-3%Cr-0.5%Mo prealloyed powder using continuous monitoring of processing-exhaust gas composition (CO, CO_2, and H_2O) were identified and interpreted in relation to density (6.5–7.4 g/cm^3), sintering temperature (1120 and 1200°C), heating and cooling rates (10 and 50°C/min), carbon addition (0.5/0.6/0.8%), type (10%H_2-N_2, N_2), and purity (5.0 and 6.0) of the sintering atmosphere. The progress in reduction processes was evaluated by oxygen and carbon contents in sintered material and fracture strength values as well. Higher sintering temperature (1200°C) and density <7.0 g/cm^3 resulted in a relative decrease of oxygen content by more than 80%. The deterioration of microclimate purity of inner microvolumes of compacts shifted the thermodynamic equilibrium towards oxidation. It resulted in a closing of residual oxides inside interparticle necks. The reducing ability of the N_2 atmosphere can be improved by sintering in a graphite container. High density of 7.4 g/cm^3 achieved by double pressing indicated a negative effect on reduction processes due to restricted replenishment of the microclimate atmosphere with the processing gas. In terms of strength properties, carbon content should not be higher than ~0.45%.

1. Introduction

Modern manufacturing techniques allow production of high-purity chromium alloyed powders [1–5] excellently predisposed to the production of structural, even highly stressed components. However, uncontrolled changes in the surface oxide composition can be obtained during sintering [6–12]. The consistent solution of this problem will mean a removal of any differences between the properties of chromium-alloyed sintered steels and most commonly used (but considerably more expensive) diffusion-alloyed powder grades.

In the literature, especially over the last 10–15 years, a lot of information and thermodynamical data on reduction reactions during sintering of Cr and Mn alloyed steels with respect to various processing conditions were presented [11–21].

The importance of several sintering parameters, like sintering temperature, type and composition of sintering atmosphere, density, carbon content, and so forth, has been widely discussed. However, there are relatively few studies systematically dealing with the influence of heating and cooling rates during sintering and particularly with the effect of green density on oxide transformation. In this way, the effect of density and pore characteristics on oxide transformation can be established as key parameters that control the redox reactions during sintering. Mitchell et al. [15, 16] and Hryha et al. [17–20] presented a thermodynamic solution for this problem, which is based on the calculation of maximum tolerable partial pressure of active components (CO, CO_2, and H_2O) in the processing gases during sintering. As pointed out by Hryha et al. [21], during sintering of powder steels alloyed with elements with a high affinity to

oxygen, special attention should be paid to the evolution of reduction/oxidation processes for the critical stage of sintering, which is the heating stage.

During sintering, depending on temperature, sintering atmosphere composition, and base material, the ongoing chemical reactions alter the composition of processing gases [22–25].

The carbothermal reduction controlled by the partial pressures of CO and CO_2 (whose ratio is controlled by Boudouard, equilibrium) plays a crucial role in the reduction of thermodynamically stable chromium oxides [25–30]. Significant knowledge of the chemical interactions during the sintering of Cr-alloyed steels has been reported by Danninger et al. [31–35]. Based on thermodynamic calculations, Hryha et al. [7, 11, 12] reported the reduction sequence of several Fe-, Cr-, Mn-, and Si-based oxides in relation to temperature:

$$\begin{aligned} Fe_2O_3 \longrightarrow FeO \longrightarrow Fe_2MnO_4 \longrightarrow Cr_2FeO_4 \longrightarrow Cr_2O_3 \\ \longrightarrow MnCr_2O_4 \longrightarrow MnO \longrightarrow MnSiO_3 \longrightarrow SiO_2 \end{aligned} \quad (1)$$

It is important to emphasize that chemical reactions occurring between the flowing furnace atmosphere and external surface of powder compacts may be quite different from the reactions that take place in the inner volume of pores of the compact, where so-called "microclimates" are formed [15]. The equilibrium state in a microclimate inside the compact is formed between carbon, oxygen, water vapour, and metallic/oxide surface of the base material. Hryha and Dudrova [19] analyzed the microclimate effect on the reduction/oxidation behaviour and on the sintering of mixed and prealloyed manganese steels. The microclimate composition which controls the reduction/oxidation processes in internal pores can only be observed indirectly. However, it has been found that at moderate density (around 7.0 g/cm^3) the furnace atmosphere, at a sufficient purity and a high flowing rate, has a significant effect on the microclimate composition [36, 37].

Hence, the contribution deals with the study of the effect of green density, sintering parameters (temperature, sintering atmosphere composition, and heating and cooling rates), and carbon content on reduction processes during sintering of the Fe-3% Cr-0.5% Mo steel powder. The influence of the above-mentioned parameters was studied by continuous analysis of evolved processing gases composition over the whole sintering cycle. Efficiency of oxide reduction was evaluated by oxygen and carbon contents in the sintered material. The effect of residual oxide on material performance was evaluated by fracture strength of sintered components.

2. Experimental Procedure

The material used in this investigation was water-atomized Fe-Cr-Mo steel powder (AstCrM, Höganäs AB, Sweden) with nominal composition of Fe-3 wt.% Cr-0.5 wt.% Mo. Chemical analysis of the AstCrM powder used is given in Table 1.

Starting powder was admixed with 0.5, 0.6, and 0.8 wt.% of carbon in the form of natural graphite Kropfmühl UF4. After homogenization of powder mixes in *Turbula* mixer, the cylindrical samples Ø10 × 12 mm^3 were compacted to densities of 6.5, 6.8, 7.1, and 7.4 g/cm^3, respectively. The density of 7.4 g/cm^3 was obtained using double pressing technique, including compaction at the pressure of 600 MPa followed by annealing at 750°C for 15 minutes in 10% H_2-N_2 atmosphere and repressing at 800 MPa. The sintering at 1120 and 1200°C for 30 min using two different heating and cooling rates, 10 and 50°C/min, was carried out in a laboratory tube furnace *ANETA 1* that allows working temperatures up to 1250°C.

Table 1: Chemical composition of AstCrM powder used.

Element	Cr	Mo	Mn	Si	Al	C	O_2	Fe
wt.%	3.0	0.48	0.037	0.089	0.025	0.019	0.197	Balance

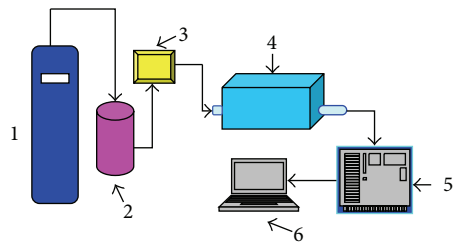

(1) Gas cylinder (10%H_2/N_2 mixture)
(2) Liquid nitrogen dryer
(3) Hygrolog (inlet dew-point)
(4) Furnace (ANETA)
(5) CO/CO_2/H_2O analyzer
(6) PC

Figure 1: Scheme of sintering atmosphere monitoring setup, sintering furnace, and PC processing of the monitored data.

The furnace constitutes a part of the sintering atmosphere monitoring setup originally installed at IMR SAS laboratory [17] (see scheme in Figure 1). Its arrangement allows in-line analysis of the exhaust gases content (CO, CO_2, and H_2O) during whole sintering cycle up to the temperature of 1200°C. The processing atmosphere used was a mixture of 10% H_2-N_2 purity 5.0 (O_2 content 1.0 ppm, H_2O content 3.2 ppm) and purity 6.0 (O_2 content 0.3 ppm, H_2O content 0.5 ppm) and N_2-atmosphere (O_2 content 1.1 ppm, H_2O content 3 ppm), from MESSER.

Particular attention was given to processing atmosphere purity that was solved by atmosphere drying using liquid nitrogen dryer. It consists of thin brass tubes immersed into a container with liquid nitrogen through which the atmosphere is blown which allows an efficient entrapment of the water vapour by its freezing. Therefore, the dew point of the inlet atmosphere, monitored by *Super-Dew SHAW* hygrolog, was −68°C. The flow rate of the atmosphere used was 2 l/min. Open ferritic stainless steel container and sampling tubes were utilized for exhaust atmosphere sampling. In each experiment, six identical samples were kept in container. The processing atmosphere was continually sampled directly from the container near the specimen surfaces using ferritic stainless tube (see Figure 2).

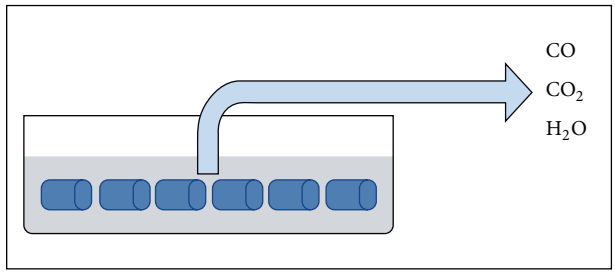

Figure 2: Scheme of sampling the atmosphere from the container.

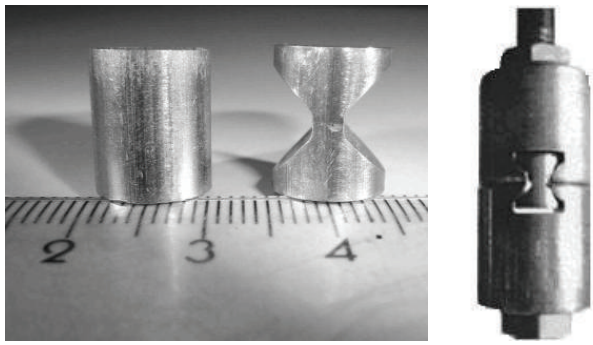

Figure 3: The shape of samples and equipment to the "button cell test."

The dew point of the sampled gases was monitored using *Michell Cermet II* sensor. CO and CO_2 contents were measured by use of nondispersed infrared analyzers on the base of *Gas Card II Plus* sensor. All sensors were connected to a PC, and continuous recording of the CO, CO_2, and H_2O contents was performed by using special software.

The powder particles surface was studied by high-resolution scanning electron microscopy (*LEO Gemini 1550*). Microstructure was observed using light (*Olympus GX 71*) and scanning electron microscopy (*Jeol JSM 7000F* coupled with *INCA EDX* analyzer). Oxygen and carbon contents in sintered components were provided using *LECO TC 36* instrument. Hereinafter presented contents of oxygen and carbon are mean values of three measurements with the spread less than 5%. The fracture strength, R_{FR}, was evaluated using nonstandard "button" tensile test method; button-shaped samples were prepared by mechanical machining of the sintered cylinders; see Figure 3.

3. Results

3.1. Surface of the Starting Powder. The surface of the water-atomized chromium pre-alloyed powder is covered by heterogeneous surface oxides composed of thin Fe-oxide layer and particulate features rich in strong oxide forming elements; see also [6–10]. In Figure 4(a), appearance of the typical surface of the starting powder is presented. Figure 4(b) shows the presence of particulate features with characteristic spherical shape and sizing up to 200 nm. Semiquantitative EDX analyses of these spherical particulates confirmed the presence of Cr, Mn, Si, Fe, and O. It is in agreement with the results of Karlsson et al. [6, 8] and Hryha et al. [9–12] that described these as thermodynamically stable complex oxides typical of the water-atomized chromium pre-alloyed powder. Distribution of oxide particles can be evaluated as more or less random, with no pronounced preference, as reported by other authors.

3.2. Effect of Density and Sintering Temperature on Reduction Processes. In Figures 5(a)–5(d) are the spectra of the processing gas composition during the whole sintering cycle at 1200°C for all the tested densities of the AstCrM + 0.5% C components. The heating rate was 10°C/min, cooling rate—50°C/min. Profile of curves of the H_2O, CO_2, and CO contents provides information on gas evolution due to respective chemical reactions and their temperature intervals during sintering. The temperature of the peaks recorded (H_2O, CO, and CO_2 profiles) and corresponding amounts of active constituent in sampled gas in relation to the density is summarized in Tables 2(a)–2(c). Other useful information on reduction processes during the heating stage and isothermal sintering is provided by the mass changes together with the oxygen and carbon contents and fracture strength listed in Tables 3 and 4.

The reduction processes take place in two temperature intervals. During the heating, the surface layer of iron oxides is reduced by hydrogen from sintering atmosphere. Carbothermal reduction of more stable oxides is theoretically possible after Boudouard's equilibrium (~720°C); however, experimentally evident reduction by graphite is observed at higher temperatures [20]. Reduction of the internal oxides is possible after dissolution of carbon in the steel matrix meaning after α-γ transformation.

The first peak on H_2O profile (Figure 5 and Table 2(a)) was observed at 180–195°C depending on the density and is connected to the removal of physically bonded water. The reduction of continuous layer of surface iron oxide (Fe_2O_3) by hydrogen starts at about ~300°C, and depending on the density it reaches a maximum at 450–513°C. This peak is also linked with the decomposition of the hydrocarbonates, created on the particle surfaces during powder handling. The peak temperature as well as the peak width clearly increases together with density. This indicates that, in the case of more dense compacts, the atmosphere penetration is restricted both ways—inwards and outwards. This corresponds to a lower amount of H_2O recorded at higher densities (see Table 2(a)). The peaks above 1000°C (1100–1196°C) are related to the reduction of iron-rich oxides from internal pores.

The reducing activity of hydrogen decreases with an increase in temperature. Further reduction processes above 700°C occurred as carbothermal reduction processes indicated by CO formation. Carbothermal reduction of iron oxides by plain carbon in Fe-C contacts reaches a maximum for densities of 6.5 and 6.8 g/cm^3 at 802°C and 820°C; for densities of 7.1 and 7.4 g/cm^3, it is 836 and 840°C.

At higher temperature, there are two maxima of CO profile: the peak at 1081°C for density 6.5 g/cm^3 and 1120°C for density 6.8 g/cm^3 and are connected with the carbothermal reduction of thermodynamically more stable surface Fe-Cr oxides and, probably, oxides from semiclosed internal

Table 2: (a) Effect of the component density on the temperature of the peaks on H_2O profile and corresponding amounts of active constituent in sampled gas. (b) Effect of the component density on the temperature of the peaks on CO profile and corresponding amounts of active constituent in sampled gas. (c) Effect of the component density on the temperature of the peaks on CO_2 profile and corresponding amounts of active constituent in sampled gas.

(a)

Density level (g/cm^3)	H_2O					
	1st peak		2nd peak		3rd peak	
	Temperature (°C)	Dew point (°C)	Temperature (°C)	Dew point (°C)	Temperature (°C)	Dew point (°C)
6.5	180	−42.4	450	−18.0	1081	−32.4
6.8	180	−41.4	470	−18.2	1126	−34.9
7.1	195	−36.9	503	−27.2	1185	−33.8
7.4	195	−36.4	513	−29.5	1184	−36.9

(b)

Density level (g/cm^3)	CO					
	1st peak		2nd peak		3rd peak	
	Temperature (°C)	Content (ppm)	Temperature (°C)	Content (ppm)	Temperature (°C)	Content (ppm)
6.5	802	180	1081	1148	1200	2234
6.8	820	109	1120	1172	1200	2205
7.1	836	219	—	—	1200	2221
7.4	840	249	—	—	1200	2218

(c)

Density level (g/cm^3)	CO_2	
	Temperature (°C)	Content (ppm)
6.5	320	139
6.8	320	154
7.1	350	201
7.4	380	115

Table 3: The mass change, oxygen and carbon contents, and fracture strength of the AstCrM + 0.5% C material heated to 730, 1120, and 1200°C and cooled at 50°C/min in relation to density.

Density level (g/cm^3)	Temperature (°C)	Sintered density (g/cm^3)	Mass change (%)	O_2 (%)	C (%)	R_{FR} (MPa)
6.5	730	6.55	0.016	0.199	0.48	—
	1120	6.55	−0.116	0.124	0.40	557
	1200	6.60	−0.225	0.069	0.36	752
6.8	730	6.89	0.003	0.209	0.48	—
	1120	6.83	−0.104	0.144	0.44	693
	1200	6.84	−0.329	0.092	0.38	731
7.1	730	7.09	−0.056	0.214	0.48	—
	1120	7.08	−0.105	0.167	0.45	704
	1200	7.12	−0.210	0.136	0.40	954

pores. With density increasing, the reduction of oxides in the core of compact becomes more difficult as the removal of reaction products from internal pores is difficult, which also corresponds to a smaller amount of CO registered for higher densities (see Table 2(b)). In the case of densities of 7.1 and 7.4 g/cm^3, the peak at 1120°C has not been recorded. As reported in [20, 21], the reduction of thermodynamically stable surface oxides Fe-Cr-Mn and iron-rich oxides from internal pores is shifted to 1120°C. Internal thermodynamically more stable Cr-Mn-Si spinel oxides typically require temperatures above 1200°C. There is only one peak at 1200°C for all tested densities. It evidently shows that with increasing density the communication of inner pores with compacts surface is restricted, and hence oxide reduction is retarded. The CO_2 peak at 320–380°C is linked with graphite oxidation as well as dissociation of the hydrocarbides, formed on the powder surface during powder handling.

The presented results obtained by monitoring the composition of processing gases are in agreement with the results obtained at degassing experiments with DTA, DTG, and mass

Table 4: Mass changes and oxygen and carbon contents in the AstCrM + 0.5% C material isothermal sintered at 1120 and 1200°C for 30 min in relation to density.

Density level (g/cm^3)	Temperature (°C)	Sintered density (g/cm^3)	Mass change (%)	O_2 (%)	C (%)	R_{FR} (MPa)
6.5	1120	6.57	−0.230	0.098	0.42	562
	1200	6.64	−0.312	0.025	0.36	838
6.8	1120	6.80	−0.297	0.097	0.42	754
	1200	6.89	−0.356	0.027	0.37	954
7.1	1120	7.11	−0.245	0.133	0.43	929
	1200	7.10	−0.291	0.068	0.39	966
7.4	1120	7.39	−0.102	0.156	0.45	416
	1200	7.39	−0.174	0.151	0.41	612

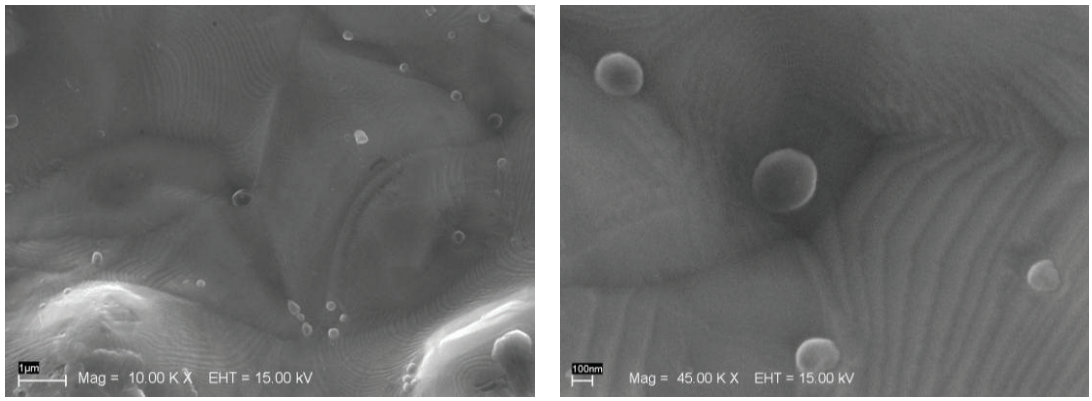

(a) (b)

Figure 4: (a) Typical surface of the AstCrM particle and (b) spherical particulate features on powder particle surface.

spectroscopy analysis as was reported by Danninger et al. [31–35].

When analyzing the changes in the mass of the compacts as well as the oxygen and carbon contents during the heating stage (Table 3) the effect of the density and temperature is evident as well. During the heating to 730°C, the mass gain was recorded for all three densities studied with corresponding relative increase in oxygen content over starting point between 1 and ~9% which also increases with density. This once again indicates more efficient reduction of the surface oxides in the case of the low-density compacts but also is affected by reoxidation during cooling stage. During the heating stage to 1120°C, as well as to 1200°C, the mass loss and oxygen content decreasing were identified for all studied densities. Lower values of the mass loss as well as lower oxygen content were obtained with increasing density confirming surface re-oxidation of the compacts during the cooling stage.

During the isothermal sintering at 1120 and 1200°C, the mass loss increased and the oxygen content decreased (see Table 4) with obvious positive effect of higher sintering temperature. Simultaneously, the negative effect of higher density on the final oxygen content that was recorded for heating stage was confirmed. The relative decrease in oxygen content over the starting point by ~50% during sintering at 1120°C was identified for densities of 6.5 and 6.8 g/cm^3; for density of 7.1 g/cm^3, it was by ~32%, and for 7.4 g/cm^3 it was only ~21%. Larger decrease in oxygen content was recorded during the sintering at 1200°C. At densities of 6.5 and 6.8 g/cm^3, it was ~87%; for density of 7.1 g/cm^3 it was ~65%, and for 7.4 g/cm^3 only 23%.

A similar trend in the development of the carbon content with increasing density is seen for both heating stage and isothermal sintering. It should be noted that such behaviour of high-density compacts is caused by employing double pressing in their preparation. As it was emphasized in [22], the most critical stage during sintering of Cr-Mn alloyed steel powders is the temperature interval around 800–900°C, as the mass transfer of the alloying elements as Cr and Mn is rather high, but thermodynamic conditions inside the pores are really poor which leads to oxide transformation from iron-based oxides to more stable Cr-Mn oxides that are difficult to reduce at typically used sintering temperatures. As repressing requires annealing at around 800°C, such oxide transformation cannot be avoided and can be only minimized by proper adjustment of the temperature, time, and atmosphere. Additionally, with the repressing with closure of residual air in the pores happens. Hence, high-density, thermodynamically more stable oxides, and closed pores cause displacement of the thermodynamic balance to

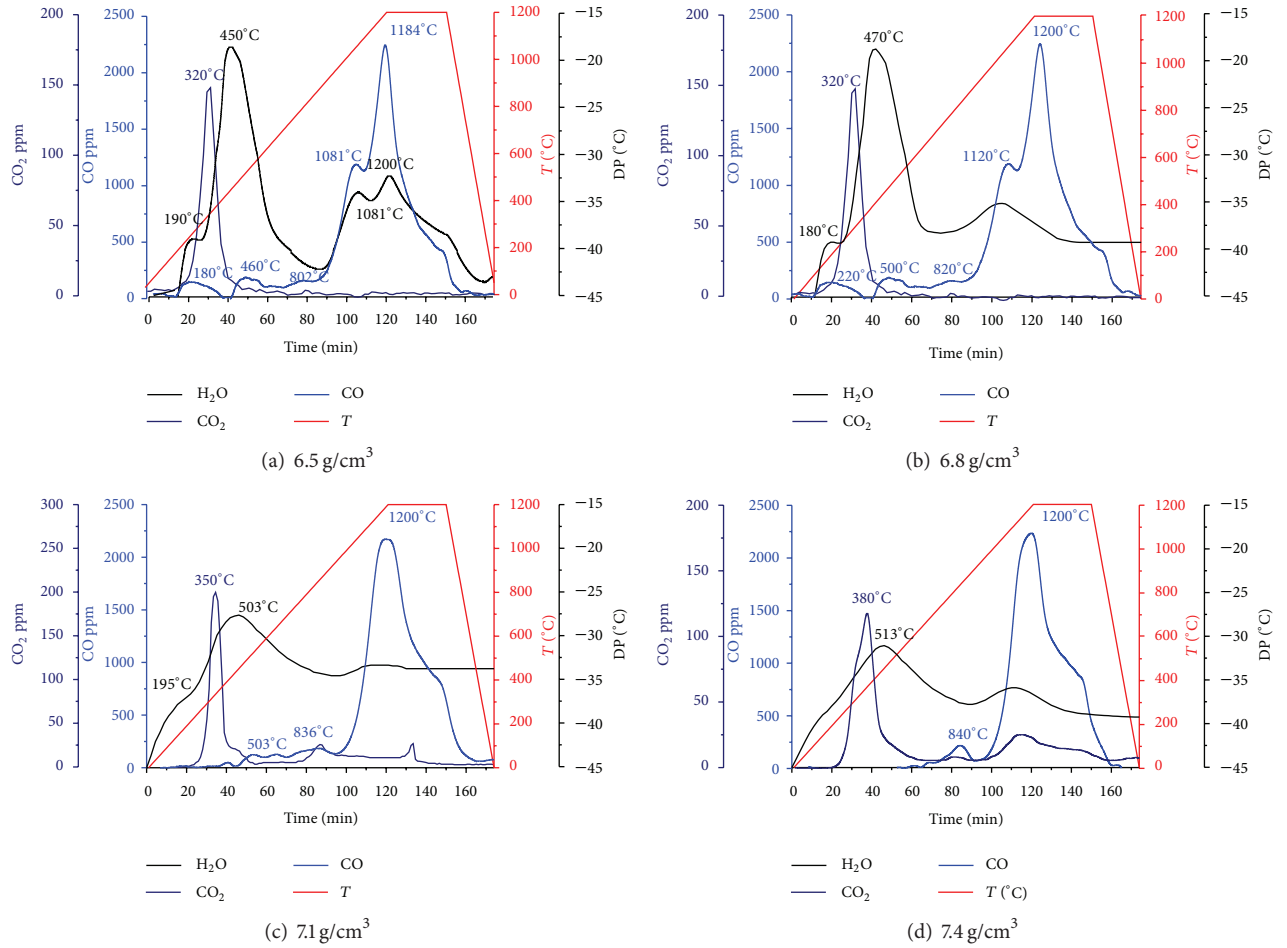

FIGURE 5: (a)–(d) Spectra of the processing gas composition monitoring during the whole sintering cycle at 1200°C of the AstCrM + 0.5% C compacts' densities of 6.5, 6.8, 7.1, and 7.4 g/cm^3, respectively.

the oxidation conditions in some microclimates which is reflected in both lower mass loss and higher oxygen content. This was also confirmed by very low decrease in oxygen content for compacts with the highest density even when sintering temperature was increased from 1120 to 1200°C that was very beneficial for lower densities.

The rate of reduction processes with positive effect of higher sintering temperature together with oxygen content reflects on the fracture strength values; see Tables 3 and 4. In accordance with higher oxygen content and thus a slower reduction processes, there has been a decrease in fracture strength at the density of 7.4 g/cm^3.

3.2.1. Oxide Inclusions in Sintered Microstructure. Micrographs in Figures 6 and 7 show a difference in the amount and arrangement of oxide particles in relation to the density and sintering temperature. For low-density compacts, the oxides are present in the form of isolated particles (see Figure 6(a)) with decreasing their number at higher sintering temperature (Figure 7(a)). At the density of 7.1 g/cm^3, the oxide contamination is slightly higher and oxides are arranged in the form of discontinuous chains along original particle surfaces. At higher sintering temperature, the amount of oxide decreases oxide chains become shorter and less continuous (Figures 6(b) and 7(b)). Evidently, a greater amount of likewise arranged oxides was found in compacts with density of 7.4 g/cm^3. As shown in Figures 7(a)–7(c), the amount and size of the oxide inclusions decrease.

The fracture surface observation of low-density components sintered at both temperatures showed the interparticle ductile failure with small equiaxed dimples initiated by carbides from bainitic microstructure and sporadically even with small oxide particles sized up to ~1 μm (see Figures 8 and 9). Higher sintering temperature led to forming structurally more improved interparticle necks with lower amount of oxide inclusions, and the failure process was accompanied with the development of local plastic flow.

This explains the increase of fracture strength values from 562 MPa to 838 MPa for sintering at the temperature of 1200°C.

For more dense compacts, the areas of interparticle ductile failure were extended, but the dimples were visibly larger and flatter. Figures 8(b) and 9(b), for failed components with density of 7.4 g/cm^3, show that shallow dimples usually

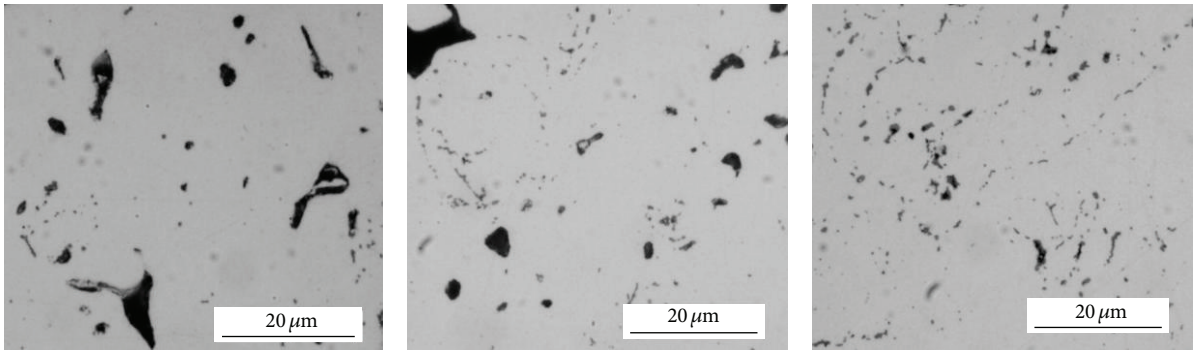

(a) (b) (c)

Figure 6: Oxide inclusions in AstCrM + 0.5% C components' densities of (a) 6.5, (b) 7.1, and (c) 7.4 g/cm^3 sintered at 1200°C for 30 min.

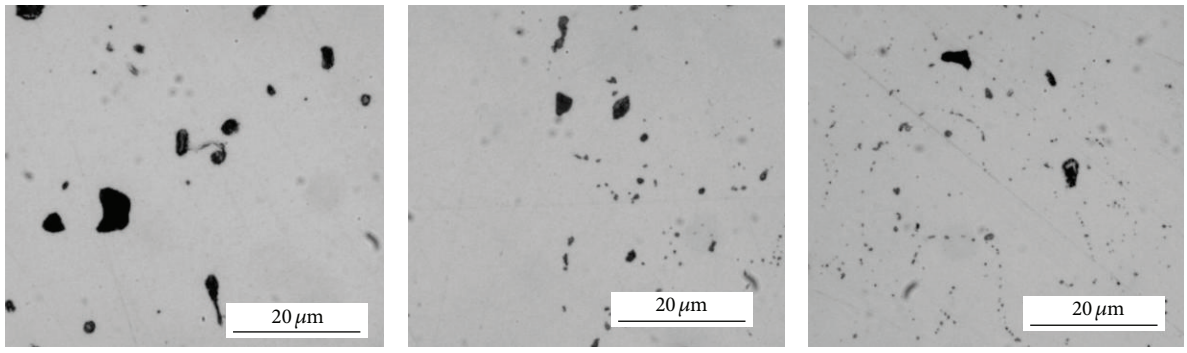

(a) (b) (c)

Figure 7: Oxide inclusions in AstCrM + 0.5% C components' densities of (a) 6.5, (b) 7.1, and (c) 7.4 g/cm^3 sintered at 1120°C for 30 min.

contain oxide inclusions or their agglomerates sized up to ~5 μm. By EDX analysis, Figure 10, the ratio of Cr : Mn in these oxide particles is close to 2 : 1, confirming that these are spinel-type oxides of Cr-Mn-Si. Higher sintering temperature led to the development of better connection, but without significant improvement in the reduction of oxides in closed microvolume of connections. The achieved fracture strength is lower that one for compacts with lower density.

3.3. Effect of Heating and Cooling Rates. In order to study the effect of heating and cooling rates on final oxygen content, two different heating and cooling rates, 10°C/min and 50°C/min, were applied. The data in Table 5 show an evident tendency for increasing oxygen content at faster heating and slower cooling rates. On the contrary, the combination of slower heating and faster cooling rate proved to be most favourable. The trend of oxygen content dependency on heating and cooling rates is maintained for all densities studied. Various combinations of heating and cooling rates during sintering at 1120°C have only low effect on relative carbon loss which was in the range from 14 to 18%. The highest value of carbon loss corresponds to density of 6.5 g/cm^3, and the lowest one to density of 7.1 g/cm^3 that, in combination with highest decrease in oxygen content observed for the same materials, indicates that highest carbon loss is associated with more efficient oxide reduction for low-density compacts by carbothermal reduction. Sintering at 1200°C leads to decrease in carbon content by 22–28%, with the lowest values for the density of 7.1 g/cm^3, as in the case of lower sintering temperature.

The values of the fracture strength in Table 5 show that the strength of the AstCrM + 0.5% C material is controlled not only by oxygen content, density, and sintering temperature, but also by cooling rate. Faster cooling rate results in the formation of mixed upper and lower bainitic structure; see Figure 11.

3.4. Effect of Purity of the Sintering Atmosphere. To evaluate the effect of purity of the sintering atmosphere on reduction of oxides in AstCrM + 0.5% C, we used the atmosphere 10% H_2-N_2 with purity 5.0 (O_2 content 1 ppm, H_2O content 3.2 ppm) and 6.0 (O_2 content 0.3 ppm, H_2O content 0.5 ppm), respectively. Two different cooling rates, 10°C/min and 50°C/min, were applied.

The data in Table 6 indicate that lower oxygen content in the atmosphere of purity 6.0 may shift the thermodynamic balance in inner microclimates toward reducing conditions more favourably than the atmosphere of purity 5.0. This resulted in efficient reduction and lower oxygen content in sintered compacts. The results also showed that the reduction

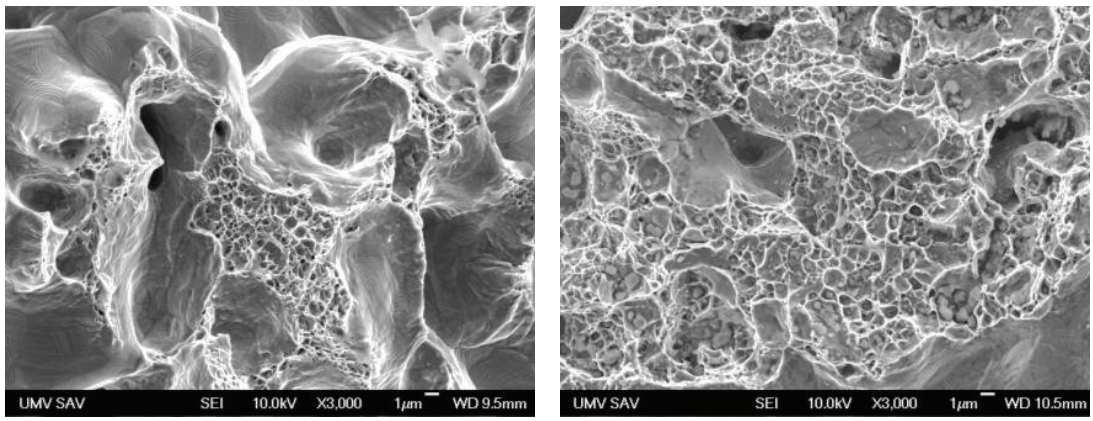

(a) (b)

Figure 8: Fracture surface of the fractured AstCrM + 0.5% C components with densities of (a) 6.5 and (b) 7.4 g/cm^3 sintered at 1120°C for 30 min.

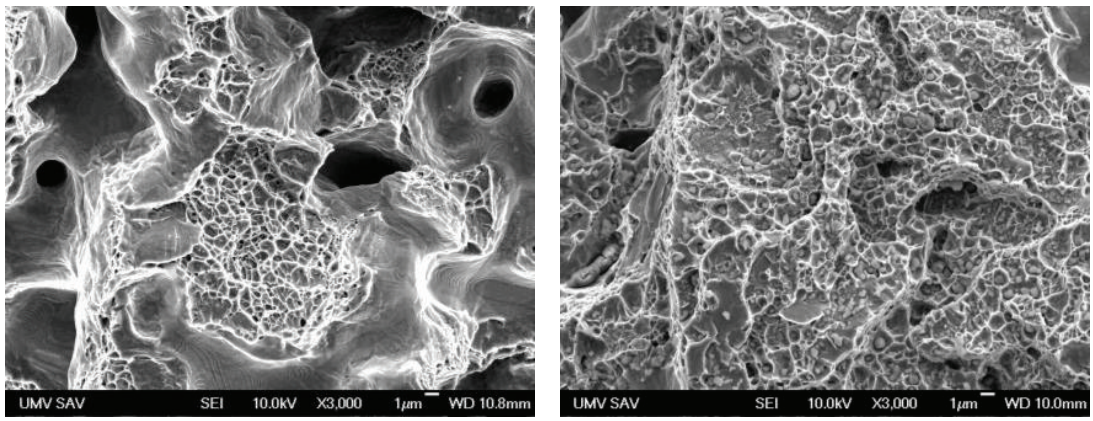

(a) (b)

Figure 9: Fracture surface of the fractured AstCrM + 0.5% C components with densities of (a) 6.5 and (b) 7.4 g/cm^3 sintered at 1200°C for 30 min.

processes are influenced by density and cooling rate as well, even when sintered in the atmosphere of purity 6.0. For compacts with a density of 6.5 g/cm^3 cooled at a higher cooling rate, a relative decrease of oxygen content over the starting point achieved the value of 64%; for densities of 6.8 and 7.1 g/cm^3, it was 54% and 37%. The atmosphere purity does not have a significant effect on carbon content and the carbon loss over the starting point ranged from 14 to 18% for all applied conditions. The positive effect of a higher purity of the sintering atmosphere on reduction processes together with a faster cooling rate resulted in higher fracture strength values; see Table 6.

3.5. Sintering in Nitrogen Atmosphere. After drying with liquid nitrogen, the AstCrM + 0.5% C compacts with densities of 6.5, 6.8, and 7.1 g/cm^3 were sintered at 1120 and 1200°C for 30 min in pure N_2-atmosphere with a dew point of −68°C.

Analyzing the spectra of H_2O, CO_2, and CO contents in exhaust gas, see Figure 12, the differences for inert and reduction atmospheres used may be identified. The H_2O curves exhibit only a small peak at 430 to 460°C that corresponds to the removal of chemically bonded water (hydroxides, hydrocarbonates, etc.). However, the amount of water vapour (the dew point from −32 to −33°C) is lower than for sintering in 10% H_2-N_2 atmosphere (see Table 2(a)). There was registered a peak at ~470°C characteristic for reduction of iron oxides by hydrogen. Similarly, the high-temperature peak at ~1100°C, which corresponds to interactions between the active gases in the system indicating further carbothermal reduction steps, has not been identified.

Small peaks on the CO curve in the range of 400–600°C are associated with decomposition of surface contaminations and graphite oxidation. The peaks above ~800°C correspond to reduction of iron oxides that are in contact with graphite. Sharpness of the peaks decreases with density increasing, as in the case of nitrogen/hydrogen blends. A tendency of peaks shifting to higher temperatures with an increase in density was registered as well. For low density of 6.5 g/cm^3, there also

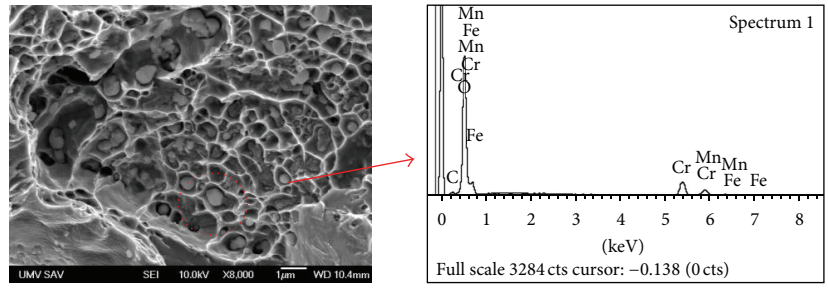

Figure 10: EDX analysis of oxides showed the presence of 34 wt.% of oxygen, 23 wt.% of chromium, and 11% of manganese and 32 wt.% of iron.

Table 5: Effect of heating and cooling rates on oxygen and carbon contents and fracture strength of AstCrM + 0.5% C material sintered at 1120 and 1200°C in relation to density.

Density level (g/cm^3)	Sintering temperature (°C)	Heating/cooling rate (°C /min)	O_2 (%)	C (%)	R_{FR} (MPa)
6.5	1120	10/10	0.114	0.41	466
		50/10	0.117	0.41	552
		10/50	0.098	0.42	640
		50/50	0.110	0.415	562
	1200	10/10	0.061	0.36	538
		10/50	0.025	0.37	838
6.8	1120	10/10	0.118	0.41	566
		50/10	0.120	0.41	620
		10/50	0.097	0.42	754
		50/50	0.108	0.42	929
	1200	10/10	0.076	0.35	725
		10/50	0.027	0.37	945
7.1	1120	10/10	0.142	0.42	719
		50/10	0.145	0.43	720
		10/50	0.133	0.43	929
		50/50	0.108	0.42	889
	1200	10/10	0.088	0.38	894
		10/50	0.068	0.38	966

Table 6: Effect of atmosphere purity and cooling rate on oxygen and carbon contents in AstCrM + 0.5% C material sintered at 1120°C for 30 min in relation to density.

Density level (g/cm^3)	Atmosphere purity	Cooling rate (°C/min)	O_2 (%)	C (%)	R_{FR} (MPa)
6.5	6.0	50	0.070	0.425	680
		10	0.095	0.41	559
	5.0	50	0.098	0.42	640
		10	0.114	0.41	466
6.8	6.0	50	0.090	0.43	788
		10	0.100	0.41	642
	5.0	50	0.097	0.42	754
		10	0.118	0.41	566
7.1	6.0	50	0.125	0.43	948
		10	0.142	0.42	801
	5.0	50	0.133	0.43	929
		10	0.142	0.42	729

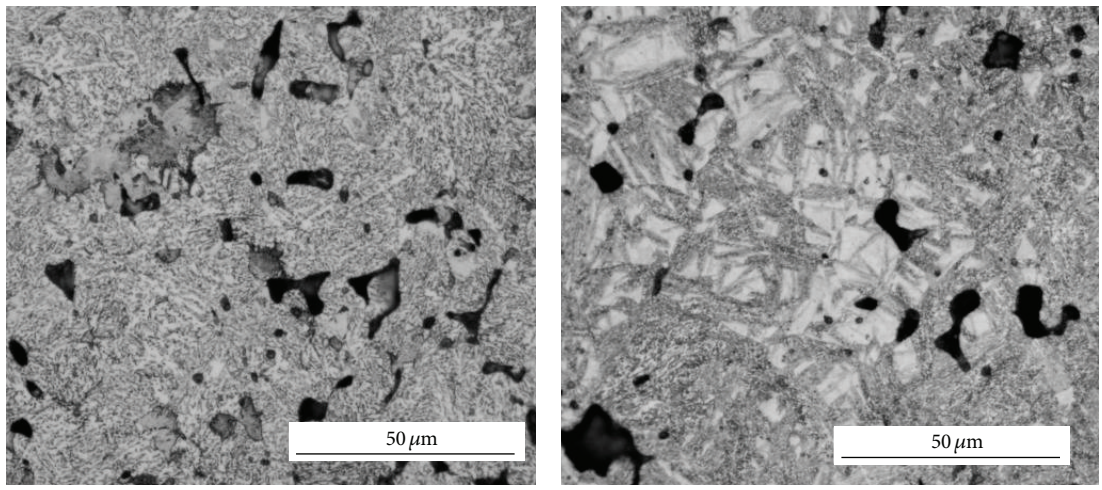

FIGURE 11: Microstructure of the AstCrM + 0.5% C components sintered at 1200°C for 30 min (a) prevalent upper bainitic when cooled at 10°C/min and upper/lower bainite mixture when cooled at 50°C/min.

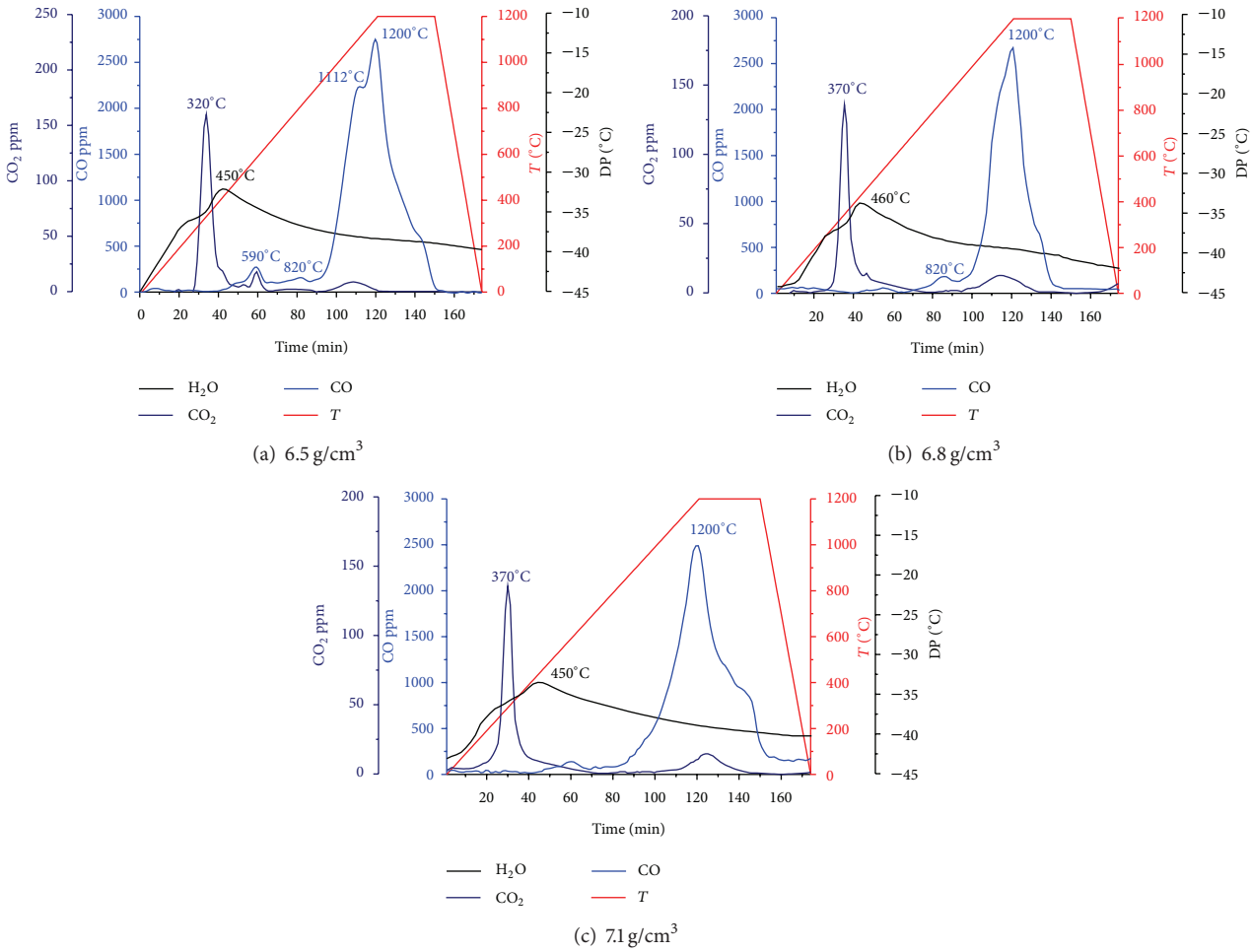

FIGURE 12: (a)–(c) Spectra of processing gas composition during sintering of the AstCr + 0.5% C components with densities of 6.5, 6.8, and 7.1 g/cm^3 at 1200°C for 30 min in N_2 atmosphere.

Table 7: Effect of sintering in N_2 atmosphere on oxygen and carbon content in the AstCrM + 0.5% C at 1120°C and 1200°C for 30 min (with heating rate of 10°C/min and cooling rates of 50°C/min) in relation to density.

Density level (g/cm^3)	Sintering temperature (°C)	O_2 (%)	C (%)	R_{FR} (MPa)
6.5	1120	0.125	0.410	537
	1200	0.044	0.360	803
6.8	1120	0.122	0.415	700
	1200	0.041	0.366	880
7.1	1120	0.136	0.430	815
	1200	0.093	0.390	943

Table 8: Oxygen and carbon contents in the AstCrM + 0.5% C components sintered at 1120°C in a graphite container using N_2 atmosphere and in a stainless container using N_2 and 10% H_2-N_2 atmospheres.

Sintering condition	O_2 (%)	C (%)	R_{FR} (MPa)
Graphite container/N_2 atmosphere	0.105	0.44	721
Stainless container/N_2 atmosphere	0.122	0.42	700
Stainless container/10% H_2-N_2	0.097	0.42	754

exists a small peak at ~1112°C corresponding to reduction of surface chromium-rich oxides and oxides from internal volumes communicating with the flowing atmosphere.

Comparing the CO profiles for sintering in pure nitrogen and H_2 containing atmosphere (see Figure 5), it is evident that the peak at ~1112°C for density of 6.5 g/cm^3 is less pronounced and the peak at ~1120°C for the density of 6.8 g/cm^3 does not appear during sintering in N_2-atmosphere at all. It enables assuming that the peak at ~1120°C is the result of H_2 and CO_2 interaction inside the sintered component. The peak with a maximum at 1200°C is associated with the carbothermal reduction of thermodynamically stable surface spinel Cr-Mn-rich oxides and mixed internal oxides. Small observed CO_2 peaks have comparable features as in the case of hydrogen-containing atmosphere.

Comparing the values in Tables 4 and 7, it can be seen that differences in carbon content resulting from sintering in N_2-atmosphere and in H_2 containing atmosphere are minimal. A tendency to increase in carbon content for specimens with higher density for both types of atmospheres is seen. Similar is also a tendency to a decreased carbon content for higher sintering temperature.

Due to a higher amount of oxides, the fracture strength after sintering in N_2 atmosphere (see Table 7) is lower than for sintering in reducing atmosphere (see Table 4).

3.5.1. Sintering in a Graphite Container in N_2 Atmosphere. The graphite container was used to increase reduction potential of carbon during sintering in N_2-atmosphere. The AstCrM + 0.5% C compacts of density 6.8 g/cm^3 were sintered at 1120°C for 30 min in a graphite container in N_2-atmosphere of purity 5.0. Comparing the oxygen content with that for sintering in a stainless container in both N_2 and H_2 containing atmospheres (see Table 8) shows that it is slightly higher than after sintering in a stainless container using H_2 containing atmosphere, but lower than for the sintering in N_2-atmosphere. At the same time the carbon content slightly increased during sintering in graphite container. Fracture strength values obtained are in a good agreement with the oxygen content.

3.6. Effect of Carbon Content Addition. The mixtures of the AstCrM powder with an addition of 0.5, 0.6, and 0.8 wt.% graphite were compacted to the density of 6.8 g/cm^3 and isothermally sintered at 1120 and 1200°C for 30 min in 10% H_2-90% N_2 atmosphere (purity of 5.0).

Analyzing the profiles of H_2O, CO_2, and CO contents and peak positions presented in Figure 13 and summarized in Table 9, it is evident that the carbon content determines the shape, temperature, and intensity of the CO peaks. The first CO peak, related to the iron oxides reduction by graphite in Fe-C contacts, was recorded at 820°C for 0.5% C; for 0.6% C it is shifted to 810°C, and for 0.8% C to 780°C. The second CO peak associated with the carbothermal reduction of stable surface chromium-rich oxides and iron oxides from the internal pores was recorded at 1120°C for 0.5% C; for 0.6% C it was shifted to 1100°C, and for 0.8% C to 1074°C.

Dew point peaks at high temperature are rather wide, and hence the peak temperature shows minimal differences in relation to carbon content. CO_2 peaks seem to be identical for materials with and without carbon addition. Low-temperature H_2O peak has a maximum at 470°C independently of graphite addition as it corresponds to the reduction of iron oxide layer by hydrogen. The CO_2 peak at 320°C was also observed in all cases, confirming that it is connected to a carbonate/hydrocarbonate decomposition and not to graphite oxidation. Some contributions from the decomposition of a small amount of the present lubricant can be expected as well.

According to oxygen and carbon contents listed in Table 10, it is shown that an increase in graphite resulted in a decrease of oxygen content by 44–51% during sintering at 1120°C and by 80–86% at 1200°C. At the same time, the carbon content decreases by 16% for sintering at 1120°C and by 30% at 1200°C. The mass changes correspond to recorded changes in oxygen and carbon contents.

The fracture strength values exhibited a decreasing tendency with an increasing carbon content. The highest strength was attested in AstCrM + 0.5% C material and the

Table 9: Temperatures of the H_2O, CO_2, and CO peaks in relation to graphite addition; AstCrM + C material with the density of 6.8 g/cm^3 sintered at 1200°C.

Graphite addition (wt.%)	H_2O peak			CO_2 peak	CO peak			
	1st (°C)	2nd (°C)	3rd (°C)	1st (°C)	1st (°C)	2nd (°C)	3rd (°C)	4th (°C)
0.5	180	470	1075	320	500	820	1120	1200
0.6	182	470	1080	320	500	810	1100	1200
0.8	170	470	1105	320	490	780	1074	1200

Table 10: Mass change and oxygen and carbon contents in AstCrM + C material with density of 6.8 g/cm^3 sintered at 1200°C in relation to graphite addition.

Graphite addition (wt.%)	Temperature (°C)	Sintered density (g/cm^3)	Mass change (%)	O_2 (%)	C (%)	R_{FR} (MPa)
0.0	1200	6.78	−0.05	0.161	—	128
0.5	1120	6.80	−0.20	0.097	0.42	754
	1200	6.89	−0.32	0.039	0.34	945
0.6	1120	6.78	−0.24	0.110	0.51	690
	1200	6.80	−0.35	0.027	0.42	847
0.8	1120	6.76	−0.29	0.110	0.68	249
	1200	6.79	−0.36	0.023	0.56	405

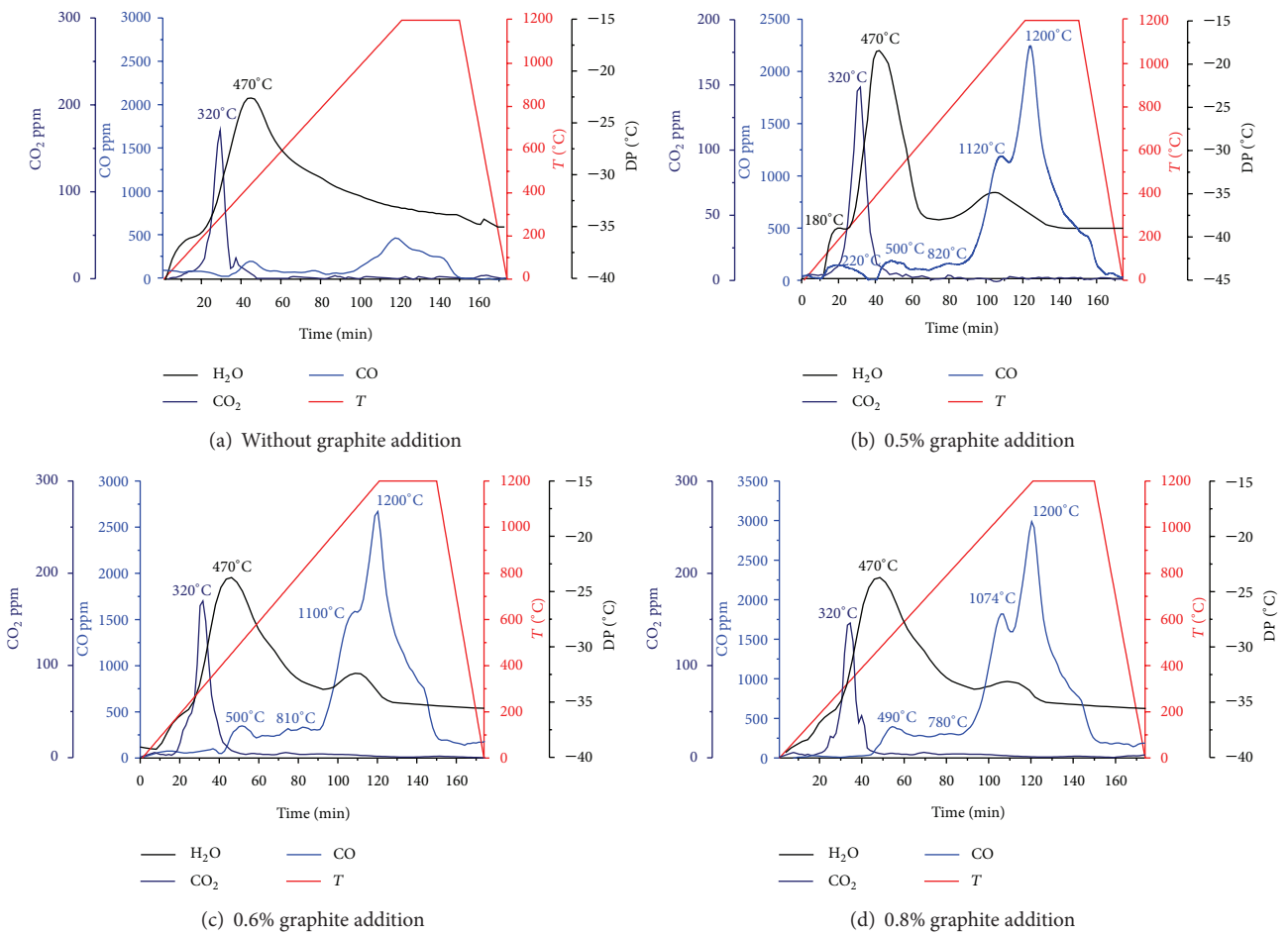

(a) Without graphite addition

(b) 0.5% graphite addition

(c) 0.6% graphite addition

(d) 0.8% graphite addition

Figure 13: (a)–(d) Spectra of sampled processing gas composition during sintering of AstCrM components without carbon and with 0.5, 0.6, and 0.8 wt.% graphite addition at 1200°C for 30 min in 10% H_2-N_2 atmosphere.

lowest for AstCrM + 0.8% C. That is caused by a higher carbon content as is eutectoid content of 0.35% at 780°C [37, 38] for the Fe-3% Cr-C system.

This is registered for AstCrM + 0.5% C material sintered at 1120°C and for all admixed with 0.6 and 0.8% C compacts; see Table 10.

Therefore, the decrease in the fracture strength is a result of the cementite film formation at grain boundaries with subsequent intergranular failure; see Figure 14 for the AstCrM + 0.8% C material.

4. Discussion

Progress in reduction processes in terms of used processing conditions (green density, sintering temperature, heating and cooling rates, type and purity of sintering atmosphere, and carbon content) has been evaluated by oxygen and carbon contents in sintered material. Effect of residual oxide contamination on material performance was analysed through fracture strength of sintered components.

Information obtained regarding achieved oxygen content and the corresponding fracture strengths for processing conditions applied in this study are summarized in Figures 15 and 16.

4.1. Oxygen Content and Processing Conditions. The highest decrease of the oxygen content in the AstCrM + 0.5% C material, more than by 75%, that is, 0.025–0.034% O_2, was achieved for low-density components (6.5 and 6.8 g/cm^3) sintered at 1200°C in 10% H_2-N_2 (5.0) atmosphere using cooling rate 50°C/min, while sintering at 1120°C resulted in a lower decrease of oxygen content, by 75–50%, that is, 0.05–0.099% O_2, for densities of 6.5 and 6.8 g/cm^3.

The use of graphite container and N_2-atmosphere for sintering of components density of 6.5 and 6.8 g/cm^3 at 1120°C with cooling at 10°C/min resulted in the decrease of oxygen content by 38–50% which represented 0.10–0.123% O_2.

The decrease in the oxygen content by 25–38% (0.123–0.148% O_2) corresponds to components density of 7.1 g/cm^3 sintered at 1120°C in both atmospheres 10% H_2-N_2 (5.0) and N_2 (5.0) and both cooling rates; higher decrease of oxygen content corresponds to higher cooling rate.

The lowest values of decrease in oxygen content, less than by 25% (i.e., oxygen content higher than 0.123%), was recorded for high-density components (7.4 g/cm^3) processed under all conditions used in this study. It should be noted that such a result is assumed to be connected to the massive oxide transformation from the iron-based to more chromium-based oxides during annealing before repressing. Additionally, such a high density results in pore enclosure inside the compact, meaning that there is limited interaction with the processing atmosphere. Poor microclimate inside the component leads to unsatisfactory surface oxides reduction. Higher oxygen content causes weakening of interfaces with oxides and therefore poor final strength properties.

4.2. Fracture Strength and Oxygen Content. Generally, as it is also evident from data in Figure 16, the strength properties of sintered steels exposed to the same loading conditions are controlled by the quality of interparticle necks (size, microstructure, and oxide contamination) and matrix microstructure, or more precisely, by micromechanical interactions of pores and microstructure of matrix surrounding the pores.

The highest values of the fracture strength, over 950 MPa, were obtained in materials with densities of 6.8 and 7.1 g/cm^3 sintered at 1200°C, which means that the main role is played by a sufficient elimination of oxides from interparticle necks, sufficiently low porosity, rounded pores, and strength bainitic microstructure. The lowest values of fracture strength, 466 to 562 MPa, belong to the low-density specimens sintered at 1120°C when, even at relatively low oxygen content of 0.098–0.125%, the negative impact of larger amount of pores dominates. The lowest fracture strength of 249 MPa is a result of grain boundaries weakened by carbidic phase at the carbon content higher than ~0.45% as well as sintering at 1120°C.

Hence, observed trends in the oxygen content development and resulting mechanical properties can be summarised as follows. Low-density components (up to 6.8 g/cm^3) can be sintered to nearly oxide-free state, even at 1120°C in hydrogen containing atmospheres, even at low purity (5.0). When it comes to the specimens with higher density (>7.0 g/cm^3), lower porosity results in restricted replenishment of the atmosphere in the local "microclimates" inside the pores and the sintering atmosphere on the surface of the compact, especially deep in the compact cores, resulting in shifting of the conditions in the pores to less reducing or even oxidising ones in comparison with lower-density compacts. As a result, oxide transformation/formation processes take place, resulting in intensive oxide formation and thus lower mechanical properties. Results also indicate that in case of repressing, special attention must be devoted during annealing treatment in order to avoid massive oxide transformation into more stable oxides—and hence interface degradation—resulting in weak interparticle necks. Therefore, importance of the sintering atmosphere purity and flow during initial stages of sintering is higher in the case of the high-density component >7.0 g/cm^3 due to the risk of oxide transformation. This is also evident in the present results, as rather low flow rate used resulted in higher oxygen content in the case of high-density components observed in other studies [39]. Results also indicate that full reduction of the oxides needs temperatures above 1200°C.

5. Conclusions

The results of the continuous monitoring of the sintering atmosphere composition confirmed that oxide reduction during sintering of Cr-alloyed water-atomized powder steels occurs in two temperature intervals. During heating in temperature interval of 300–500°C, reduction of surface iron oxides by hydrogen from sintering atmosphere occurs. Carbothermal reduction connected to CO formation starts above 750°C. The reduction of stable surface Fe-based mixed

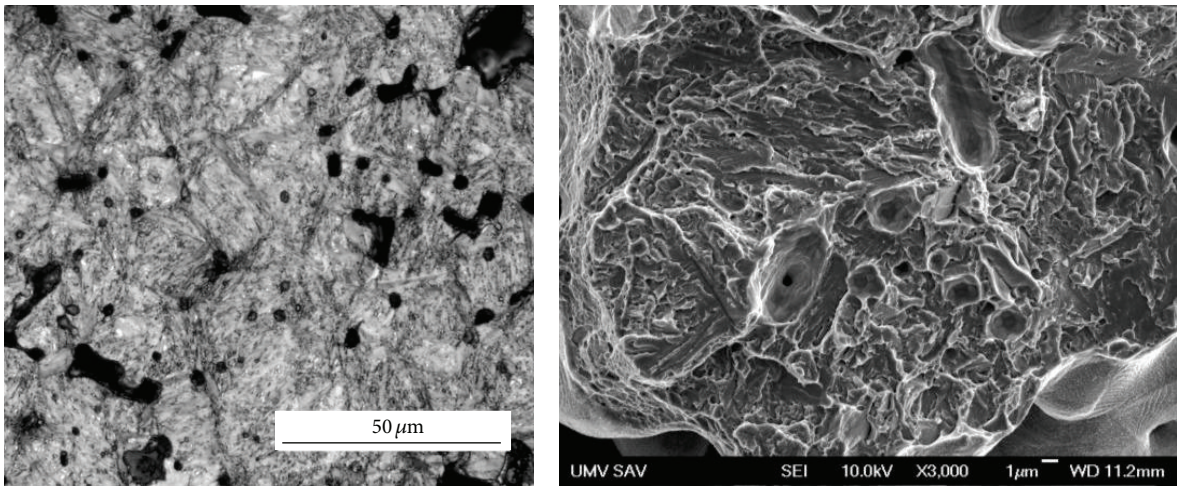

(a) (b)

Figure 14: Microstructure and fracture surface of AstCrM + 0.8% C material sintered at 1200°C.

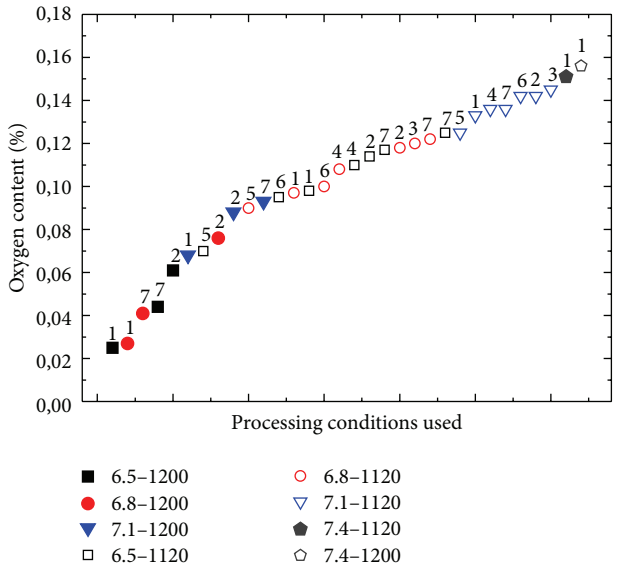

Figure 15: Oxygen content increasing in AstCrM-C alloys in relation to the processing conditions used.

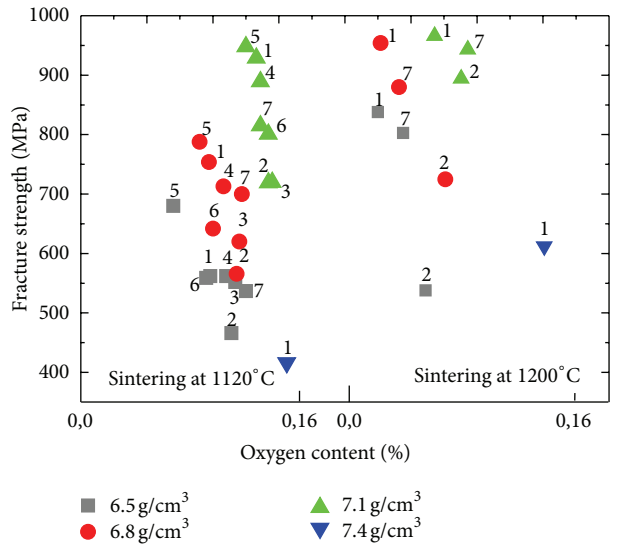

Figure 16: Fracture strength in relation to oxygen content achieved at processing condition used.

oxides, where Mn and Cr may be present, but in diluted form, takes place above 1000°C. Stable Mn-Cr-rich surface oxides and internal oxides are reduced at about 1200°C.

Oxide reduction processes are more advanced after sintering at a higher temperature (1200°C) which results in lower oxygen content. Evidently, the use of 1200°C as compared to 1120°C represents a more favourable condition for oxide reduction not only thermodynamically but also kinetically. This has also been recently confirmed in a work by Danninger [35].

The oxygen content increases with density of material sintered at both temperatures of 1120 and 1200°C. With a green density increasing, the reduction processes become more difficult due to poor interaction of the atmosphere inside the pores of the compact—"microclimate"—with the sintering atmosphere on the compact surface, and the reduction processes are shifted to higher temperatures.

Faster heating rate (50°C/min) has a negative effect on reduction processes due to insufficient "blow off" of reduction gas products. Hence, higher flow has to be combined with the corresponding flow rate, high enough to assure full removal of reduction products. Deterioration of the purity of the atmosphere in the inner microvolumes of compacts shifts the thermodynamical equilibrium towards oxidation, and it results in enclosure of residual oxides inside particle necks. The consequence of oxide enclosure is higher oxygen content and lower mechanical properties of the compacts.

Using higher cooling rate can prevent reoxidation of material during the cooling stage. The results confirmed

the advantage of hydrogen containing atmosphere when hydrogen reduces iron oxide layer early during the heating stage. Hydrogen also contributes to the increasing of reduction ability of microclimates within compacts at high temperatures through water reaction.

The results confirmed that different carbon contents has a minor effect on reduction processes, but, as it is well known, the carbon content has a significant effect on microstructure. To achieve the desired performance, the carbon content in AstCrM-C material has to be below eutectoid content in as-sintered state. The optimal carbon content for AstCrM is 0.40–0.45 wt.%; a higher content negatively impacts the strength properties. As previously reported by Ortiz and Castro [28], PM steels in this alloy system, with carbon contents higher than 0.45 wt.%, are hypereutectoid.

Acknowledgment

The authors are grateful for the financial support of Slovak National Grant Agency (Project VEGA 2/0153/12).

References

[1] S. Berg and B. Maroli, "Properties obtained by chromium contained material," in *Advances in Powder Metallurgy and Particulate Materials*, V. Arnhold, C. L. Chu, W. F. Jandeska Jr., and H. I. Sanderow, Eds., part 8, pp. 1–14, MPIF, Princeton, NJ, USA, 2002.

[2] A. Bergmark, J. Andersson, and S. Bengston, "Chromium pre-alloyed PM steels for high structural performance," in *Proceedings of the EURO PM2005 Conference*, vol. 1, pp. 157–152, EPMA, Prague, Czech Republic, 2005.

[3] U. Engstrom, D. Milligan, and A. Klekovkin, "Mechanical properties of high performance chromium materials," in *Advances in Powder Metallurgy & Particulates Materials*, vol. 7, pp. 21–32, MPIF, San Diego, Calif, USA, 2004.

[4] A. Bergmark, O. Bergman, and L. Alzati, "Pre-alloyed chromium materials for highly fatigue loaded PM parts," in *Advanced in Powder Metallurgy & Particulates Material*, part 2, pp. 13–21, MPIF, Chicago, Ill, USA, 2004.

[5] M. Hull, "Astaloy CrM new generation powder from Höganäs," *Powder Metallurgy*, vol. 41, no. 4, pp. 232–233, 1998.

[6] H. Karlsson, *Role of surface oxides in sintering of chromium-alloyed steel powder [Ph.D. thesis]*, Chalmers University of Technology, Goteborg, Sweden, 2005.

[7] E. Hryha and L. Nyborg, "Oxide transformation during sintering of pre-alloyed water atomized steel powder," in *Proceedings of the PM2010 Powder Metallurgy World Congress & Exhibition*, vol. 2, pp. 267–274, Florence, Italy, 2010.

[8] H. Karlsson, L. Nyborg, and S. Berg, "Surface interaction during sintering of water-atomized pre-alloyed steel powder," in *Proceedings of the World Congress & Exhibition on Powder Metallurgy*, vol. 2, pp. 22–23, EPMA, Vienna, Austria, 2004.

[9] E. Hryha, C. Gierl, L. Nyborg, H. Danninger, and E. Dudrova, "Surface composition of the steel powders pre-alloyed with manganese," *Applied Surface Science*, vol. 256, no. 12, pp. 3946–3961, 2010.

[10] E. Hryha, L. Nyborg, and S. Bengston, "Surface analysis of pre-alloyed with manganese steel powder," in *Proceedings of the PM2010 World Congress and Exhibition*, vol. 2, pp. 169–174, EPMA, Florence, Italy, 2010.

[11] D. Chasoglou, E. Hryha, and L. Nyborg, "Effect of sintering atmosphere on the transformation of surface oxides during the sintering of chromium alloyed steels," *Powder Metallurgy Progress*, vol. 9, no. 3, pp. 141–147, 2009.

[12] D. Chasoglou, E. Hryha, and L. Nyborg, "Surface interactions during sintering of chromium-alloyed PM steels in different atmospheres," in *Proceedings of the PM2010 World Congress and Exhibition*, vol. 2, pp. 45–52, EPMA, Florence, Italy, 2010.

[13] O. Bergman, B. Lindqvist, and S. Bengtsson, "Influence of sintering parameters on the mechanical performance of PM steels pre-alloyed with chromium," *Materials Science Forum*, vol. 534–536, no. 1, pp. 545–548, 2007.

[14] O. Bergman, *Study of oxide reduction and nitrogen uptake in sintering of chromium-alloyed steel powder [Licentiate Thesis]*, 2008.

[15] S. C. Mitchell and A. Cias, "Carbothermic reduction of oxides during nitrogen sintering of manganese and chromium steels," *Powder Metallurgy Progress*, vol. 4, no. 3, pp. 132–142, 2004.

[16] M. Youseffi, S. C. Mitchell, A. S. Wronski, and A. Cias, "Sintering, microstructure, and mechanical properties of PM manganese-molybdenum steels," *Powder Metallurgy*, vol. 43, no. 4, pp. 353–358, 2000.

[17] E. Hryha, *Fundamental study of Mn containing PM steels with alloying method of both premix and pre-alloy [Ph.D. thesis]*, IMR SAS, Košice, Slovakia, 2007.

[18] E. Hryha, L. Cajkova, and E. Dudrova, "Study of reduction-oxidation processes in Cr-Mo pre alloyed steels during sintering by continuous atmosphere monitoring," *Powder Metallurgy Progress*, vol. 7, no. 4, pp. 181–189, 2008.

[19] E. Hryha and E. Dudrova, "The sintering behaviour of Fe-Mn powder system, correlation between thermodynamics and sintering process, manganese distribution and microstructure composition, effect of alloying mode," in *Application of Thermodynamics to Biological and Materials Science*, M. Tadashi, Ed., vol. 22, pp. 573–602, InTech, Rijeka, Croatia, 2011.

[20] E. Hryha, E. Dudrova, and L. Nyborg, "On-line control of processing atmospheres for proper sintering of oxidation-sensitive PM steels," *Journal of Materials Processing Technology*, vol. 212, no. 4, pp. 977–987, 2012.

[21] E. Hryha, L. Nyborg, C. Gierl, H. Danninger, and S. Bengtsson, "Surface analysis of prealloyed steel powders: qualitative and quantitative aspects," in *Proceedings of the PM2010 World Congress and Exhibition*, vol. 1, pp. 25–32, EPMA, Florence, Italy, 2010.

[22] E. Hryha and L. Nyborg, "Changes in oxide chemistry during consolidation of Cr/Mn water atomized steel powder," *Powder Metallurgy Progress*, vol. 11, no. 1-2, pp. 42–50, 2011.

[23] E. Mosca, "Controlled atmospheres in powder metallurgy, in sintering theory and practice," Intensive Short Course, EPMA, Torino, Italy, 1996.

[24] P. Beiss, "Sintering atmospheres for PM steels," in *Proceedings of the Höganäs Chair in Powder Metallurgy Workshop Sintering Atmospheres*, Vienna, Austria, 1999.

[25] G. F. Bocchini, "Influence of controlled atmospheres on the proper sintering of carbon steels," *Powder Metallurgy Progress*, vol. 4, no. 1, pp. 1–34, 2004.

[26] J. Ardvidsson, "On-line measurement of sintering atmospheres," in *Proceedings of the World Congress PM98*, vol. 2, pp. 253–260, EPMA, Grenada, Spain, 1998.

[27] P. Ortiz and F. Castro, "Thermodynamic and experimental study of role of sintering atmospheres and graphite additions

on oxide reduction in Astaloy CrM powder compacts," *Powder Metallurgy*, vol. 47, no. 3, pp. 291–298, 2004.

[28] P. Ortiz and F. Castro, "Study of gas solid interactions during sintering of Cr-containing PM steels," in *Proceedings of the PM2003 Conference*, vol. 1, pp. 243–248, EPMA, Valencia, Spain, 2003.

[29] L. M. Berger, S. Stolle, W. Gruner, and K. Wetzig, "Investigation of the carbothermal reduction process of chromium oxide by micro- and lab-scale methods," *International Journal of Refractory Metals and Hard Materials*, vol. 19, no. 2, pp. 109–121, 2001.

[30] W. Gruner, S. Stolle, and K. Wetzig, "Formation of CO_x species during the carbothermal reduction of oxides of Zr, Si, Ti, Cr, W, and Mo," *International Journal of Refractory Metals and Hard Materials*, vol. 18, no. 2, pp. 137–145, 2000.

[31] H. Danninger and C. Gierl, "Processes in PM steel compacts during the initial stages of sintering," *Materials Chemistry and Physics*, vol. 67, no. 1-3, pp. 49–55, 2001.

[32] H. Danninger, C. Gierl, S. Kremel, G. Leitner, and K. Jaenicke-Roessler, "Degassing during sintering of different Fe and Fe-0.8%C powder compacts," in *Proceedings of the PM World Congress Sintering (PM98)*, vol. 2, pp. 342–346, EPMA, Grenada, Spain, 1998.

[33] H. Danninger, C. Gierl, S. Kremel, G. Leitner, K. Jaenicke-Roessler, and Y. Yu, "Degassing and deoxidation process during sintering of unalloyed and alloyed PM steels," *Powder Metallurgy*, vol. 2, no. 3, pp. 125–139, 2002.

[34] H. Danninger, C. Gierl, S. Kremel, G. Leitner, and K. Jaenicke-Roessler, "A simple method to study the degassing and reduction processes during sintering of ferrous powder compacts," *P/M Science & Technology Briefs*, vol. 6, no. 3, pp. 10–14, 2004.

[35] H. Danninger, C. Xu, and B. Lindqvist, "Oxygen removal during sintering of steels prepared from Cr-Mo and Mo prealloyed powders," *Materials Science Forum*, vol. 534–536, no. 1, pp. 577–580, 2007.

[36] M. Hrubovcakova, *Microchemistry of interfaces in sintered microstructure of sintered high-strength steels [Ph.D. thesis]*, IMR SAS, Košice, Slovakia, 2011.

[37] M. Hrubovcakova, E. Dudrova, and J. Harvanova, "Influence of carbon content on oxide reduction during sintering of Cr-Mo-C pre-alloyed steel," *Powder Metallurgy Progress*, vol. 11, no. 1-2, pp. 115–122, 2011.

[38] M. Dlapka, *Sinterhardening grade steels with sufficient toughness for synchronizer hub applications [Ph.D. thesis]*, TU, Vienna, Austria, 2011.

[39] O. Bergman, *Key aspect of sintering powder metallurgy steel pre-alloyed with chromium and manganese [Ph.D. thesis]*, Chalmers University of Technology, Gothenburg, Sweden, 2011.